Design and Implementation of Novel Single-Stage Charge-Pump Power Factor Correction Electronic Ballast for Metal Halide Lamp

Ray-Lee Lin and Chih Lo
Department of Electrical Engineering, National Cheng-Kung University, Tainan City, TAIWAN.
raylin@ieee.org

***Abstract*--This paper presents a novel single-stage charge-pump (CP) power-factor-correction (PFC) electronic ballast for the MH lamps driven with the low-frequency square-wave current to avoid the acoustic-resonance problem. In order to achieve high power factor and meet the IEC regulation, the CPPFC technique is applied to the full-bridge inverter of the conventional electronic ballast. Based on the analyses of the operational modes for the proposed electronic ballast, the design criteria of the CP components for the proposed electronic ballast are presented. A prototype circuit for 35-W MH lamp is implemented to confirm the presented design criteria.**

Keywords: Charge-pump (CP), power-factor-correction (PFC), single-stage, metal halide lamp, electronic ballast.

I. INTRODUCTION

Recently, the metal halide (MH) lamp has become an attractive lighting source because of its good color rendering, compact size, and high luminous efficiency [1-3]. However, the MH lamp has the phenomenon of acoustic resonance, which causes arc fluctuation, visible flicker, and damage of arc tube [4-7]. In order to avoid the acoustic-resonance problem, driving the MH lamp with low-frequency square waveform current is an excellent solution [7].

The block diagram of the conventional two-stage electronic ballast for the MH lamp is shown in Fig. 1 [8-10]. The first stage, a boost converter, is the power factor correction (PFC) stage, which is used to achieve high power factor and provide a constant DC bus voltage to the second stage. The second stage is a full-bridge inverter, which is utilized to adjust the lamp power and drive the MH lamp with the low-frequency square wave current.

In order to simplify the conventional electronic ballasts and meet the power factor regulations, many single-stage charge-pump power factor correction (CPPFC) schemes for electronic ballasts have been studied and developed [11-15]. The voltage source (VS) CPPFC electronic ballast for fluorescent lamp and the equivalent circuit are shown in Fig. 2(a) and Fig. 2(b), respectively [15]. According to the designs for the parameters of the CP components C_{in1}, C_{in2} and L_{r1} in [15], the input current can be shaped into sinusoidal waveform to meet the requirements of high power factor.

In this paper, the CPPFC technique is applied to the full-bridge inverter of the conventional electronic ballast for the single MH lamp. Comparing the conventional electronic ballast, the power switch and the control circuit of the PFC stage can be saved. Consequently, the developed single-stage electronic ballast has potentially cost-effective advantage.

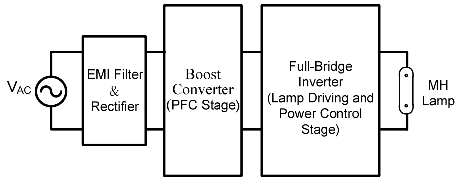

Fig. 1. Block diagram of conventional two-stage electronic ballast for MH lamp [10].

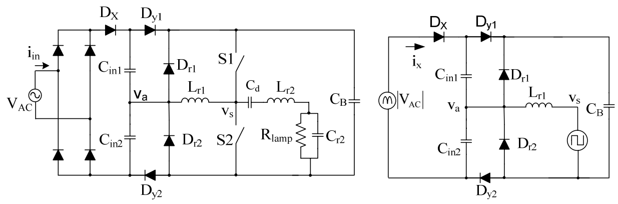

Fig. 2. (a) VS-CPPFC converter and (b) equivalent circuit of VS-CPPFC converter [15].

II. PROPOSED ELECTRONIC BALLAST

Fig. 3 shows the proposed single-stage CPPFC electronic ballast for the MH lamps. In the CPPFC network, the CP components L_X, C_{in1} and C_{in2} are utilized to shape the line current into sinusoidal waveform to meet the requirements of IEC 61000-3-2 Class-C Standard. The resonant inductor L_r of the CPPFC network is used to reduce the current stress on the switches S_{H1} and S_{H2} and the diodes D_{r1}, D_{r2}, D_{y1}, and D_{y2}. In addition, the resonant inductor L_x is used to improve the input power factor of the electronic ballast.

The key waveforms of the proposed electronic ballast are shown in Fig. 4, where the switches S_{H1} and S_{H2} of the full-bridge inverter are operated with high-frequency pulse width modulation (PWM). In addition, the switches S_{L1} and S_{L2} of the full-bridge inverter are operated complementarily at low-frequency with 50% duty ratio. With the operations of the full-bridge inverter and rectified line voltage, the operational

978-1-4244-5226-2/10/$26.00 ©2010 IEEE

modes of the electronic ballast can be divided to intervals Ⅰ, Ⅱ, Ⅲ, and Ⅳ.

Fig. 5 shows the block diagram of the control circuit for the proposed electronic ballast. The line-voltage sensing circuit is used to detect the line voltage for the MCU. When the sensed signal $v_z(t)$ from the line-voltage sensing circuit reaches zero level, the MCU begins to provide the low-frequency clock signals $V_{g,SL1}$ and $V_{g,SL2}$ with the twice line frequency for the low-frequency half-bridge driver. Furthermore, the MCU also provides the high-frequency clock signal V_{HF} to modulate the operating frequency of the PWM controller.

The current-sensing level-shifting technique [16-17] is employed to achieve the constant lamp power for the proposed electronic ballast. The duty ratio of the signal V_{PWM} can be controlled with the sensed signal $v_{cs(t)}$, which is the sum of the feedback signals $v_{lv}(t)$ and $v_{ic}(t)$. Then, the signal V_{PWM} from the PWM controller is fed into the high-frequency half-bridge driver to generate $V_{g,SH1}$ and $V_{g,SH2}$ by comparing with the signal $V_{g,SL2}$.

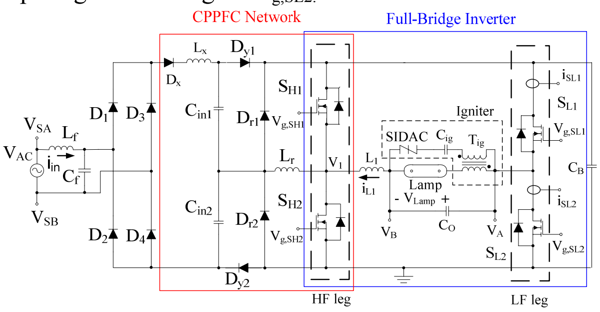

Fig 3. Proposed single-stage CPPFC electronic ballast for MH Lamp.

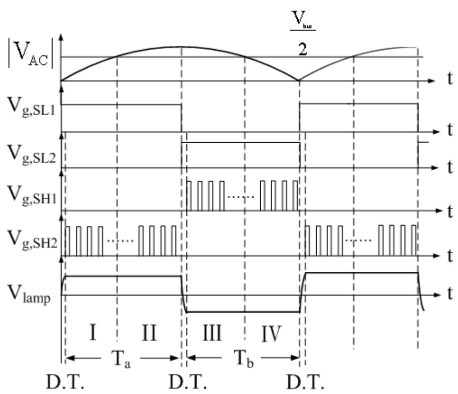

Fig. 4. Key waveforms of proposed electronic ballast.

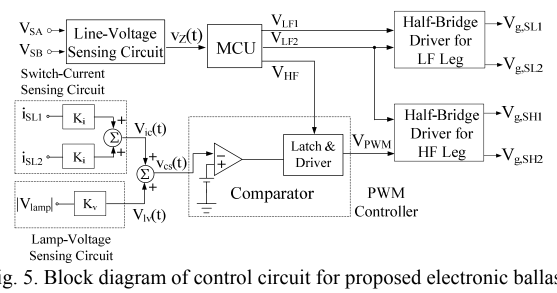

Fig. 5. Block diagram of control circuit for proposed electronic ballast.

III. Operational Principles

The operational principals of the electronic ballast in Interval-Ⅱ are analyzed in this paper. The equivalent circuit and the key waveforms of the proposed electronic ballast in Interval-Ⅱ are shown in Fig. 6 and Fig. 7, respectively. Fig. 8 shows the detailed key waveforms for the duration T_{a2} shown in Fig.7. Within one high-frequency switching cycle, the operational modes in Internal-Ⅱ include eleven topological stages, as shown in Fig. 9. Referring to the Fig. 7, 8 and 9, the operational principles of the eleven topological stages in interval-Ⅱ are described as follows.

Mode-1 [$t_0 \sim t_1$]: At $t=t_0$, the switch S_{H2} is turned on. The DC-bus voltage V_{bus} is applied to the C_O-R_{lamp}-L_1 network. Therefore, the inductor current i_{L1} increases linearly. Meanwhile, the capacitor C_{in2} discharges to the resonant inductor L_r. When the capacitor voltage v_{Cin2} decreases to the rectified line voltage $|V_{AC}|$ at t_1, the diode D_X conducts.

Mode-2 [$t_1 \sim t_2$]: The CP capacitor C_{in2} is discharged by the net current between the inductor currents i_{Lr} and i_X. When the voltage v_{Cin2} across the capacitor C_{in2} reaches zero at t_2, the clamping diode D_{r2} conducts.

Mode-3 [$t_2 \sim t_3$]: The inductor L_X and the capacitor C_{in1} are charged by the line input current while the voltage level V_{Cin1} is lower than rectifier line voltage $|V_{AC}|$. The capacitor C_{in1} is charged by the inductor current i_X until the voltage v_{Cin1} reaches the DC bus voltage V_{bus}.

Mode-4 [$t_3 \sim t_4$]: The diodes D_{y1} and D_{y2} conduct at t_3. The energy stored in the inductor L_X is released to the bulk capacitor C_B. Since the value of rectified line voltage $|V_{AC}|$ is lower than the DC bus voltage V_{bus}, the inductor current i_X decreases linearly.

Mode-5 [$t_4 \sim t_5$]: The body diode D_{SH1} of the switch S_{H1} conducts while the switch S_{H2} is turned off at t_4. The energies stored in the inductors L_r and L_X transfer to the bulk capacitor C_B. In addition, the inductor L_1 discharges to the capacitor C_O and the resistor R_{lamp}. When the inductor current i_X decreases to zero, this mode ends.

Mode-6 [$t_5 \sim t_6$]: The energy stored in inductors L_r is released to the bulk capacitor C_B until the inductor current i_{Lr} reaches zero.

Mode-7 [$t_6 \sim t_7$]: The diode D_{y1} conducts while the diode D_{r2} is turned off at t_6. The capacitor C_{in1} discharges to the inductor L_r. The inductor current i_{Lr} decreases until the negative value of the inductor current i_{Lr} equals to the value of the inductor current i_{L1}.

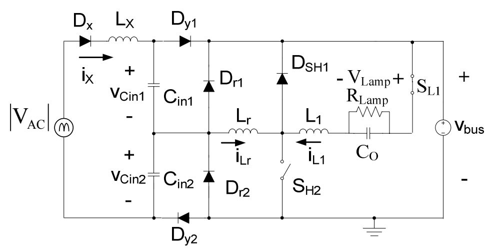
Fig. 6. Equivalent circuit of proposed electronic ballast in Internal-Ⅱ.

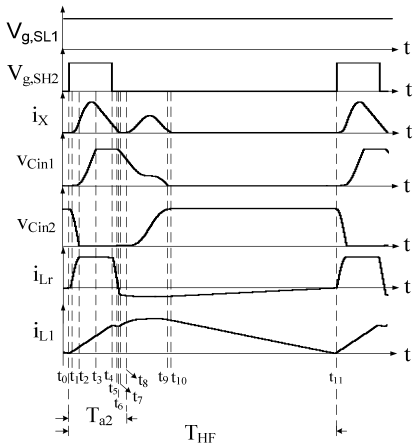

Fig. 7. Key waveforms of proposed electronic ballast in Interval-Ⅱ.

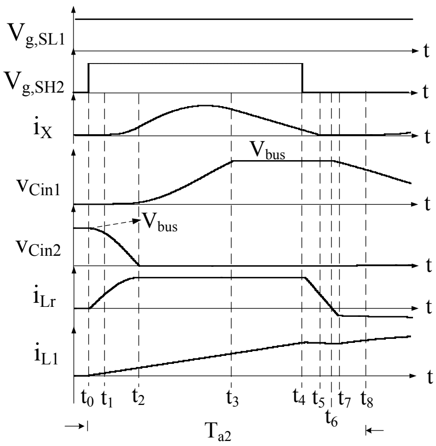

Fig. 8. Detailed key waveforms of Fig. 7 in duration T_{a2}.

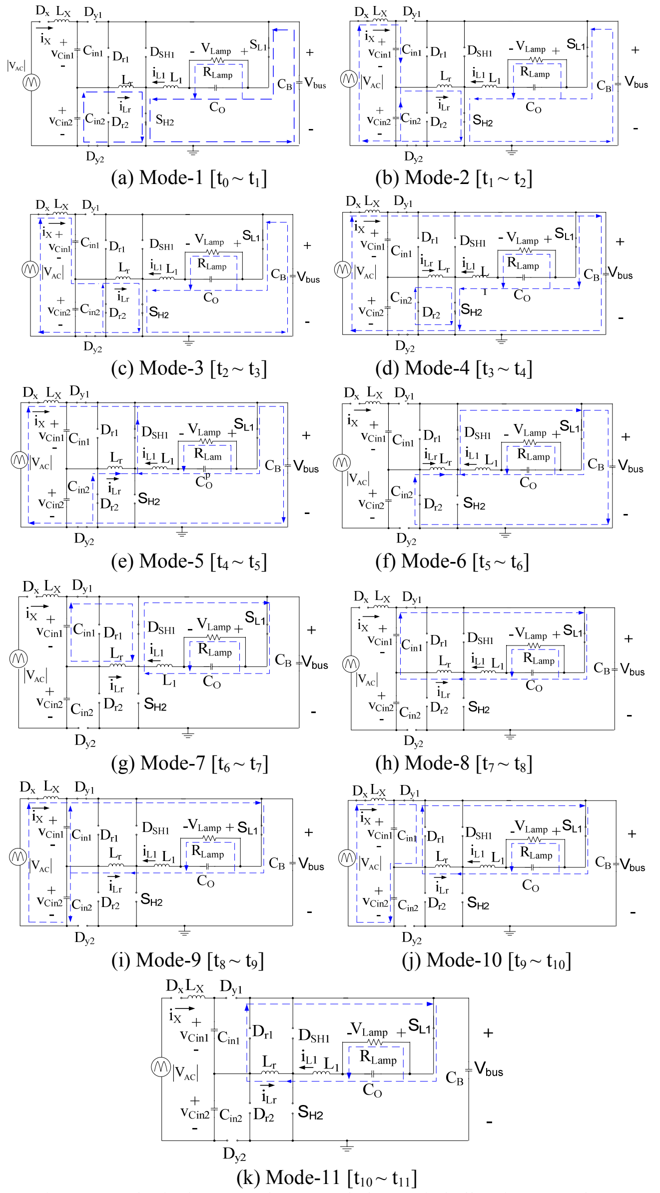

Fig. 9. Topological stages of proposed electronic ballast in Interval-Ⅱ.

Mode-8 [$t_7 \sim t_8$]: Since the voltage level of the capacitor C_{in1} is higher than the lamp voltage V_{lamp}, the CP capacitor C_{in1} discharges to the C_O-R_{lamp}-L_1-L_r network. Therefore, the voltage V_{Cin1} decreases and the inductors currents i_{L1} and i_{Lr} increase. When the voltage V_{Cin1} reaches the rectified line voltage $|V_{AC}|$ at t_8, the diode D_X conducts.

Mode-9 [$t_8 \sim t_9$]: The CP capacitor C_{in1} discharges to the C_O-R_{lamp}-L_1-L_r network. Besides, the inductor L_X and capacitors C_{in1}, C_{in2} are charged by the line input current while the voltage level across the capacitors C_{in1}, C_{in2} is lower than rectifier line voltage $|V_{AC}|$. The capacitor C_{in1} is charged by the difference current between the inductor currents i_{L1} and i_X until the voltage v_{Cin1} reaches zero at t_9.

Mode-10 [$t_9 \sim t_{10}$]: The inductors L_r and L_1 discharge to the resistor R_{lamp} and capacitor C_O. The inductor currents i_{L1} and i_{Lr} decreases linearly. The capacitor C_{in2} is charged by the inductor current i_X until the inductor current i_X reaches zero at t_{10}.

Mode-11 [$t_{10} \sim t_{11}$]: The inductors L_r and L_1 discharge to the capacitor C_O and resistor R_{lamp}. When the inductor currents i_{L1} and i_{Lr} reach zero at t_{11}, the switch S_{H2} is turned on and the next high-frequency switching cycle begins.

IV. Design Guidelines

In order to simplify the derivation for the expression of the line current, the following assumptions are made:

- Steady-state operation and constant DC bus voltage,
- switches and diodes are ideal components,
- values of CP capacitors C_{in1} and C_{in2} are specified the same,
- resonant inductor L_r is neglected,
- i_{L1} during Mode-9 in Interval-Ⅱ are assumed as a constant current source.

The equivalent circuits to represent the conducting paths of the inductor current i_X are shown in Fig. 10. And Fig. 11 shows the key waveforms of the equivalent circuits to represent the conducting paths of the inductor current i_X.

Mode-3 [$t_{a0} \sim t_{a1}$]

According to the equivalent circuit to represent the conducting path of the inductor current i_X during Mode-3 illustrated in Fig. 10(a), the inductor current $i_x(t)$ and the capacitor voltage $v_{Cin1}(t)$ can be obtained, as shown in Equations (1) and (2), respectively.

$$i_x(t) = \frac{|V_{AC}|}{Z_{X1}} \cdot \sin\left[\omega_{X1}(t - t_{a0})\right], \quad (1)$$

$$v_{Cin1}(t) = |V_{AC}| - |V_{AC}| \cos\left[\omega_{X1}(t - t_{a0})\right], \quad (2)$$

where

$$Z_{X1} = \sqrt{\frac{L_X}{C_{in1}}} \text{ ,and}$$

$$\omega_{X1} = \frac{1}{\sqrt{L_X \cdot C_{in1}}}.$$

Mode-4 through Mode-5 [$t_{a1} \sim t_{a2}$]

According to the equivalent circuit to represent conducting path of the inductor current i_X during Mode-4 and Mode-5, as shown in Fig. 10(b), the inductor current $i_x(t)$ can be obtained, as shown in Equation (3).

$$i_x(t) = \frac{(|V_{AC}| - V_{bus})(t - t_{a1})}{L_X} + \frac{\sqrt{2|V_{AC}| \cdot V_{bus} - V_{bus}^2}}{Z_{X1}}. \quad (3)$$

Mode-9 [$t_{a3} \sim t_{a4}$]

According to the equivalent circuit to represent the conducting path of the inductor current i_X in Mode-9, as shown in Fig. 10(c), the inductor current $i_x(t)$ and the capacitor voltages $V_{Cin1}(t)$, $V_{Cin2}(t)$ can be obtained, as shown in Equations (4), (5), and (6), respectively.

$$i_X(t) = \frac{i_{L1}(t_{a3})}{2} - \frac{i_{L1}(t_{a3}) \cdot \cos\left[\sqrt{2}\omega_{X1}(t - t_{a3})\right]}{2}, \quad (4)$$

$$v_{Cin1}(t) = |V_{AC}| - \frac{i_{L1}(t_{a3}) \cdot (t - t_{a3})}{2 \cdot C_{in1}} - \frac{\sqrt{2} \cdot Z_{X1} \cdot i_{L1}(t_{a3}) \sin\left[\sqrt{2} \cdot \omega_{X1}(t - t_{a3})\right]}{4}, \quad (5)$$

$$v_{Cin2}(t) = \frac{i_{L1}(t_{a3}) \cdot (t - t_{a3})}{2C_{in1}} - \frac{\sqrt{2} \cdot i_{L1}(t_{a3}) \cdot Z_{X1} \cdot \sin\left[\sqrt{2} \cdot \omega_{X1}(t - t_{a3})\right]}{4}, \quad (6)$$

where $i_{L1}(t_{a3})$ is the initial value of the inductor current i_{L1} at t_{a3}.

Mode-10 [$t_{a4} \sim t_{a5}$]

According to the equivalent circuit to conducting path of the inductor current in Mode-10, as shown in Fig. 10(d), the inductor current $i_x(t)$ can be obtained, as shown in Equation (7).

$$i_x(t) = i_x(t_{a4}) \cdot \cos\left[\omega_{X1}(t - t_{a4})\right] + \frac{|V_{AC}|}{Z_{X1}} \cdot \sin\left[\omega_{X1}(t - t_{a4})\right] - \frac{v_{Cin2}(t_{a4})}{Z_{X1}} \sin\left[\omega_{X1}(t - t_{a4})\right], \quad (7)$$

where $i_x(t_{a4})$ and $v_{Cin2}(t_{a4})$ are the initial values of the inductor current i_X and the capacitor voltage v_{Cin2} at t_{a4}, respectively.

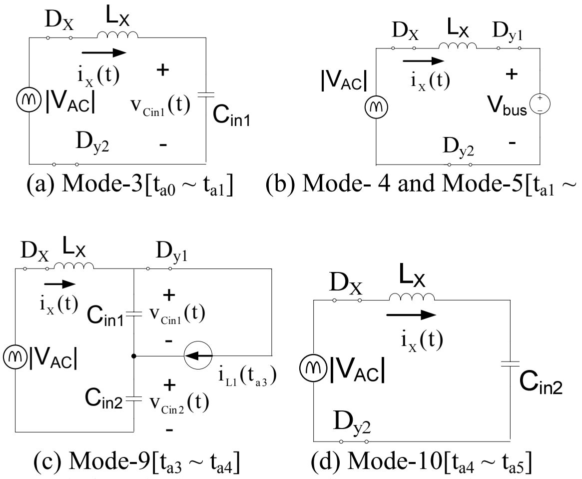

(a) Mode-3[$t_{a0} \sim t_{a1}$] (b) Mode- 4 and Mode-5[$t_{a1} \sim t_{a2}$]

(c) Mode-9[$t_{a3} \sim t_{a4}$] (d) Mode-10[$t_{a4} \sim t_{a5}$]

Fig.10. Equivalent circuits to represent line current paths of proposed electronic ballast in Interval-Ⅱ.

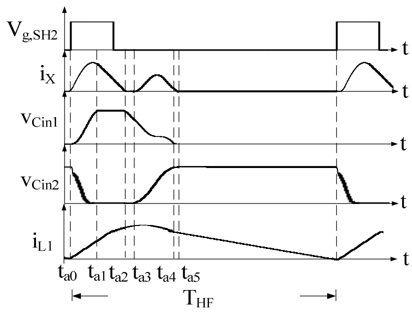

Fig. 11. Key waveforms for equivalent circuits to represent conducting paths of inductor current i_X

According to the preceding analysis, the average line current i_{in_avg} over one high-frequency switching cycle in Interval-Ⅱ can be obtained as shown in Equation (8).

$$i_{in\_avg} = i_{X\_avg} = \frac{1}{T_{HF}}\left[\int_{t_{a0}}^{t_{a2}} i_X(t)dt + \int_{t_{a3}}^{t_{a5}} i_X(t)dt\right]. \quad (8)$$

By substituting Equations (1), (3), (4), and (7) into Equation (8), the average line current equation in Interval-Ⅱ can be rewritten, as shown in Equation (9).

$$i_{in\_avg} = \frac{1}{T_{HF}}\left[K_1 \cdot \left|V_{AC}\right| + K_2 + K_3 + K_4\right], \quad (9)$$

where $K_1 = C_{in1} \cdot (2 - \cos(\omega_{X1} \cdot T_{A\_1}) - \cos(\omega_{X1} \cdot (T_{A\_4}))$,

$$K_2 = \frac{C_{in1} \cdot V_{bus} \cdot (2 \cdot \left|V_{AC}\right| - V_{bus})}{2(V_{bus} - V_{AC})},$$

$$K_3 = \frac{i_{L1}(t_{a3}) \cdot T_{A3}}{2} - \frac{\sin(\sqrt{2}\omega_{X1} \cdot T_{A\_3})}{2 \cdot \omega_{X1}},$$

$$K_4 = \frac{i_x(t_{a4}) \cdot \sin(\omega_{X1} \cdot T_{A\_4})}{\omega_{X1}} + v_{Cin2}(t_{a4}) \cdot C_{in1}(1 - \cos(\omega_{X1} T_{A\_4})),$$

$T_{A\_1} = t_{a1} - t_{a0}$,

$T_{A\_3} = t_{a4} - t_{a3}$, and

$$T_{A\_4} = t_{a5} - t_{a4}.$$

Based on the energy conservation between the input power and output power, Equation (10) can be obtained as follows:

$$\frac{P_O}{\eta} = V_{AC\_rms} \cdot I_{in\_rms} = \frac{V_{AC\_pk} \cdot I_{in\_pk}}{2} \tag{10}$$

where

P_o is the lamp power,

η is the conversion efficiency,

V_{ac_pk} is the peak value of the line voltage, and

i_{in_pk} is the peak value of the line current.

Based on Equation (9) and Equation (10), the expression of the CP capacitor C_{in1} can be derived, as shown in Equation (11).

$$C_{in1} = (1.23 \cdot 10^4 \cdot K_a + 111K_a\sqrt{(1.23 \cdot 10^4 \cdot K_a + 6.57 \cdot 10^4 \cdot K_b + 4 \cdot 10^4 \cdot K_c)} + 3.28 \cdot 10^4 \cdot K_b - 2 \cdot 10^4 \cdot K_c) \times \frac{50(V_{AC\_pk} - V_{bus})}{\left[K_d - 500V_{bus}^2\right]^2 V_{AC\_pk} \cdot \eta} \tag{11}$$

where $K_a = V_{AC\_pk} \cdot \eta \cdot L_X \cdot i_{L1}(t_{a3})^2 (V_{AC\_pk} - V_{bus})$,

$K_b = T_{HF} \cdot P_O \cdot L_X \cdot i_{L1}(t_{a3})(V_{AC\_pk} - V_{bus})$,

$K_c = T_{HF} \cdot P_O \cdot V_{bus}^2$, and

$K_d = 821 \cdot L_X \cdot i_{L1}(t_{a3})(V_{AC\_pk} - V_{bus})$.

At $t = \frac{\pi}{2 \cdot \omega_{X1}} + t_{a0}$, Equation (1) can be rewritten as Equation (12) in order to calculate the inductor peak current i_{X_pk}.

$$i_{X\_pk} = \sqrt{\frac{C_{in1}}{L_X}} \cdot V_{AC\_pk}. \tag{12}$$

Combining Equations (11) and (12), the expression of the inductance L_X can be derived, as shown in Equation (13).

$$L_X = \frac{\eta^2 \cdot C_{in1} \cdot V_{AC\_pk}^4}{4 \cdot P_O^2 \cdot K_e^2}, \tag{13}$$

where

$$K_e = \frac{i_{X\_pk}}{i_{in\_pk}}.$$

The specifications for the proposed electronic ballast are listed in Table 1.Plotted from Equation (11), Fig. 12 shows the relationship between the values of the CP capacitors C_{in1}, C_{in2} and the DC-bus voltage V_{bus} with different values of inductor L_X. Fig. 12 shows that the DC-bus voltage V_{bus} increases as the values of the CP capacitors C_{in1} and C_{in2} increase.

Plotted from Equation (13), Fig. 13 shows the relationship between the value of inductor L_X versus the value of CP capacitors C_{in1} and C_{in2} with different value for factor K_e. According to Fig. 13, the value of inductor L_X increases as the values of the CP capacitors C_{in1} and C_{in2} increase.

By applying η=0.8, V_{bus}=380V, K_e=5, $i_{L1}(t_{c3})$=0.796 A, and the specifications in Table 1 to Equations (11) and (13), the value of the CP capacitors C_{in1}, C_{in2} and the value of the inductor L_X can be calculated as 4.37nF and 312μH, respectively.

Table 1. Specifications of prototype circuit.

Specifications	Values
Input AC Voltage V_{AC}	200 V_{rms} to 242 V_{rms}, at 60Hz
Rated Lamp Voltage V_{Lamp}	88V_{rms}
Rated Lamp Current I_{Lamp}	398mA
Rated Lamp Power P_{Lamp}	35W
Operating Frequency of LF Leg f_{LF}	120 Hz
Switching Frequency of HF Leg f_{HF}	50 kHz

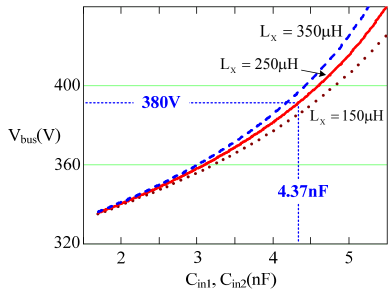

Fig. 12. Relationship between value of the CP capacitors C_{in1}, C_{in2} and DC-bus voltage.

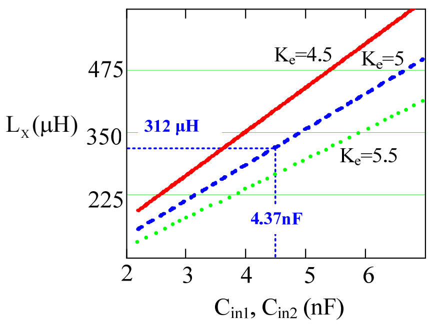

Fig. 13. Relationship between value of inductor L_X versus value of CP capacitors C_{in1} and C_{in2} with different factor K_e.

V. EXPERIMENTAL RESULTS

Based on the specifications and the parameters, listed in Tables 1 and 2, respectively, a prototype circuit for 35W MH lamp is implemented to validate the presented design criteria.

Fig. 14 shows the measured waveforms of the input voltage and the input current at 220 V_{rms} input voltage. Fig. 15 illustrates the comparison between the measured input current harmonic and the IEC 61000-3-2 Class-C Standard. The measured PF and THD are 0.976 and 16.3%, respectively.

In Fig. 16, the lamp voltage and current waveforms at steady-state are 88.7 V_{rms} and 409 mA, respectively. Fig. 17 shows the photo of the shaking-free arc in the MH lamp. The measured efficiency is between 74.4% and 78.9% when the input AC voltage V_{AC} ranges from $200V_{rms}$ to $242V_{rms}$.

Table 2. Parameters of prototype circuit.

Components	Description	Components	Description
S_{L1}, S_{L2}	K2843/600V	C_{in1}, C_{in2}	4.4nF
S_{H1},S_{H2}	2SK2625/600V	C_{bus}	47uF
L_x	305μH	C_o	330nF
L_r	55 μH	D_x, D_{y1}, D_{y2}	MUR 160/600V
L_1	1.2mH	D_{r1}, D_{r2}	MUR 260/600V

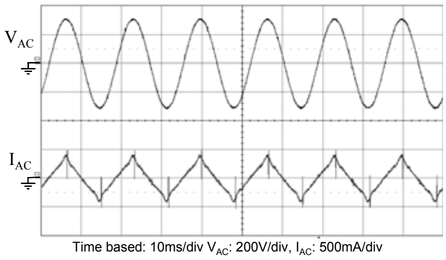

Fig. 14. Measured waveforms of input voltage and input current at 220 V_{rms} AC input voltage.

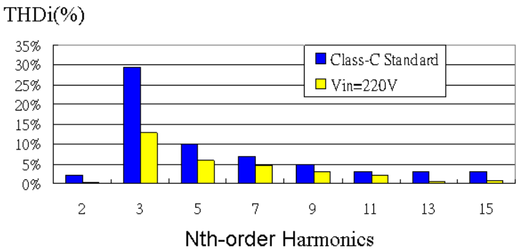

Fig. 15. Measured input current harmonics and IEC 61000-3-2 Class-C Standard.

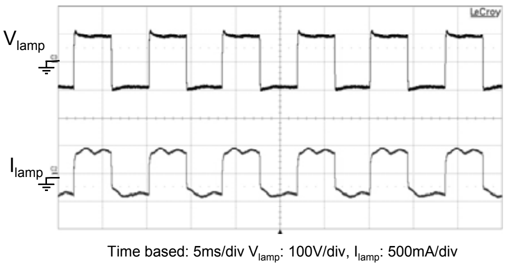

Fig. 16. Measured waveforms of lamp voltage and lamp current.

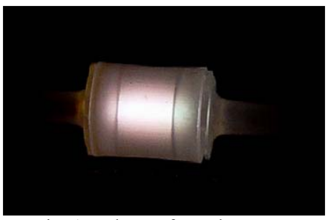

Fig. 17. Photo of MH lamp arc.

VI. Conclusions

A novel single-stage CPPFC electronic ballast for the MH lamp has presented in this paper. Based on the operational principles of the proposed electronic ballast, the design equations for the CP components L_X, C_{in1} and C_{in2} have been presented to calculate the parameters of the proposed electronic ballast. A prototype circuit for 35W MH lamp has been designed and implemented. The input current harmonics meet the IEC 61000-3-2 Class-C Standard. The PF is 0.976 and the THD is 16.3%, respectively.

Acknowledgement

This work was sponsored by the National Science Council, Taiwan, under Award Numbers NSC 97-2221-E-006-275-MY2 and 99-2221-E-006-231. Also, this work made use of Shared Facilities supported by the Program of Top 100 Universities Advancement, Ministry of Education, Taiwan.

References

[1] B. Cook, “New developments and future trends in high-efficiency lighting,” *Eng. Sci. Educ. J.*, vol. 9, no. 5, pp. 207-217, 2000.

[2] M. Sugiura, “Review of metal-halide discharge-lamp development 1980-1992,” in *Proc. IEE Meas., Technol.*, Vol. 140, No. 6, Nov. 1993, pp. 443-449.

[3] C. S. Moo, S. Y. Tang, C. R. Lee, J. H. Chen, and W. T. Tsai, “Investigation into high-Frequency operating characteristics of metal-halide lamps,” *IEEE Trans. Power Electron.*, vol. 37, no.11, pp. 2234-2240, Nov. 2009.

[4] M. Ponce, A. Lopez, J. Correa, J. Arau and J. M. Alonso, “Electronic ballast for HID lamps with high frequency square waveform to avoid acoustic resonances,” in *Proc. IEEE APEC’01*, 2001, vol. 2, pp.658-663.

[5] C. A. Cheng, T. J. Liang, C. M. Chuang, and J.F. Chen, "A high power factor electronic ballast of projector lamps with variable frequency control," in *Proc. IEEE PESC’02*, 2002, vol. 1, pp. 213-217.

[6] W. Yan, Y. K. E. Ho, and S. Y. R. Hui, “Stability study and control methods for small-wattage high-intensity-discharge (HID) lamps,” *IEEE Trans. Ind. Appl.*, vol. 37, no. 5, pp. 1522-1530, Sep./Oct. 2001.

[7] M. A. Dalla Costa, J. M. Alonso, J. Garcia, J. Cardesin, and M. Rico-Secades, “Acoustic resonance characterization of low-wattage metal halide lamps under low-frequency square-waveform operation,” *IEEE Trans. Power Electron.*, vol. 22, no. 3, pp. 735-743, 2007.

[8] M. Shen, Z. Qian, and F. Z. Peng, “Design of a two-stage low-frequency square-wave electronic ballast for HID lamps,” *IEEE Trans. Ind. Appl.*, vol. 39, no. 2, pp. 424-430, Mar./Apr. 2003.

[9] F. J. Diaz, F. J. Azcondo, R. Casanueva, C. Branas, R. Zane, "Digital control of a Low-Frequency Square-Wave electronic ballast with resonant ignition," IEEE Tran. on Ind. Electron., vol. 55, no. 9, pp. 3180-3191, September. 2008.

[10] T. J. Liang, C. M. Huang, and J. F. Chen, “Interleaving controlled three-leg electronic ballast for dual-HID-lamps.” IEEE Trans. on Power Electronics, vol. 23, no. 3, May 2008, pp. 1401-1409.

[11] J. Qian and F. C. Lee, “Voltage-source charge-pump power-factor-correction ac-dc converters,” IEEE Trans. on Power Electronics, vol. 14, no. 2, pp. 350–358, Mar. 1999.

[12] R. L. Lin, H.Y. Liu, and H. M. Shih, “AC-side CCM CS-CP-PFC Electronic Ballast,” IEEE Trans. on Power Electronics, vol. 22, no. 3, May 2007, pp. 789-796.

[13] J. Qian, F. C. Lee, and T. Yamauchi, “Current-source charge-pump power-factor-correction electronic ballast,” *IEEE Trans. Power Electron.*, vol. 13, no. 3, pp. 564-572, May 1998.

[14] J. Qian, F. C. Lee, and T. Yamauchi, “New continuous-input current charge pump power-factor-correction electronic ballast,” *IEEE Trans. Power Electron.*, vol. 35, no. 2, pp. 433-441, Mar./Apr. 1999.

[15] J. Qian, "Advanced Single-Stage Power Factor Correction Techniques," Ph.D. Dissertation, Virginia Tech, September 1997.

[16] C. M. Huang, T. J. Liang, R. L. Lin, and J. F. Chen, “Constant power control circuit for HID electronic ballast,” in *Proc. IEEE IAS Annu. Meeting*, 2005, pp. 1193-1197.

[17] C. M. Huang, T. J. Liang, R. L. Lin, and J. F. Chen, “A novel constant power control circuit for HID electronic ballast,” *IEEE Trans. Power Electron.*, vol. 22, no. 3, pp. 854-862, 2007.